Science of the Total Environment 942 (2024) 173713

Contents lists available at ScienceDirect

Science of the Total Environment

journal homepage: www.elsevier.com/locate/scitotenv

Anthropogenic-driven changes in concentrations and sources of winter volatile organic compounds in an urban environment in the Yangtze River Delta of China between 2013 and 2021

Zihang Zhang [a], Yunjiang Zhang [a,*], Sheng Zhong [b,*], Jie Fang [a], Baoru Bai [c], Cheng Huang [d,*], Xinlei Ge [a]

[a] Collaborative Innovation Center of Atmospheric Environment and Equipment Technology, Jiangsu Key Laboratory of Atmospheric Environment Monitoring and Pollution Control, School of Environmental Science and Engineering, Nanjing University of Information Science and Technology, Nanjing, China
[b] Jiangsu Environmental Monitoring Center, Nanjing, China
[c] Sinopec Engineering Incorporation, Beijing, China
[d] Shanghai Environmental Monitoring Center, Shanghai, China

HIGHLIGHTS

- Significant winter VOCs decline in urban Nanjing due to effective anthropogenic emission control.
- Substantial shifts in VOCs sources reflect changing energy consumption patterns.
- Strictly reducing VOC emissions from vehicles should be prioritized for health exposure considerations.

GRAPHICAL ABSTRACT

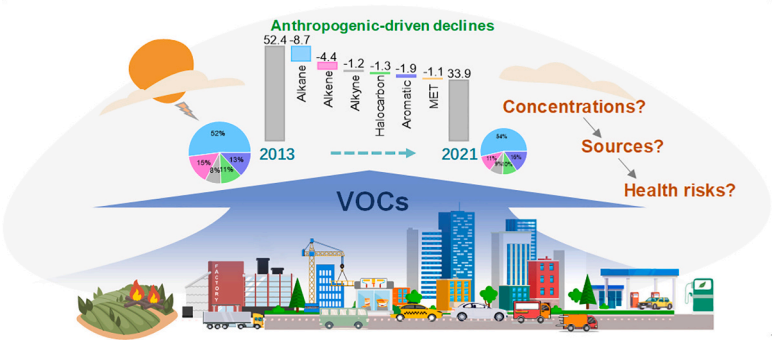

ARTICLE INFO

Editor: Meng GAO

Keywords:
VOCs
Source apportionment
Clean air actions
Machine learning
Yangtze River Delta

ABSTRACT

Volatile organic compounds (VOCs) serve as crucial precursors to surface ozone and secondary organic aerosols (SOA). In response to severe air pollution challenges, China has implemented key air quality control policies from 2013 to 2021. Despite these efforts, a comprehensive understanding of the chemical composition and sources of urban atmospheric VOCs and their responses to emission reduction measures remains limited. Our study focuses on analyzing VOCs composition and concentrations during the winters of 2013 and 2021 through online field observations in urban Nanjing, a typical city in the Yangtze River Delta region of China. Using a machine learning approach, we found a notable reduction in total VOCs concentration from 52.4 ± 30.4 ppb to 33.9 ± 21.6 ppb between the two years, with dominant contributions (approximately 94.3 %) associated with anthropogenic emission control. Furthermore, alkanes emerged as the major contributors (48.6 %) to such anthropogenic-driven decline. The total SOA formation potential decreased by approximately 27.4 %, with aromatics identified as the major contributing species. Positive matrix factorization analysis identified six sources.

* Corresponding authors.
E-mail addresses: yjzhang@nuist.edu.cn (Y. Zhang), zhongs@jshb.gov.cn (S. Zhong), huangc@saes.sh.cn (C. Huang).

https://doi.org/10.1016/j.scitotenv.2024.173713
Received 31 March 2024; Received in revised form 28 May 2024; Accepted 31 May 2024
Available online 5 June 2024

In 2013, prominent contributors were solid fuel combustion (43.6 %), vehicle emission (16.7 %), and paint and solvent use (12.8 %). By 2021, major sources shifted to solid fuel combustion (31.9 %), liquefied petroleum gas and natural gas (26.8 %), and vehicle emission (25.5 %). Solid fuel combustion emerged as the primary driver for total VOCs reduction. The lifetime carcinogenic risk in 2021 decreased by 72.6 % relative to 2013, emphasizing the need to address liquefied petroleum gas and natural gas source, and vehicle emissions for improved human health. Our findings contribute critical insights for policymakers working on effective air quality management.

1. Introduction

Volatile organic compounds (VOCs) are important atmospheric pollutants that play a crucial role in the formation of tropospheric ozone (O_3) (Atkinson, 2007; de Gouw et al., 2005; Wang et al., 2020b; Li et al., 2021). Their interaction with nitrogen oxides (NOx) significantly influences the production of ozone (Atkinson, 2000). Additionally, VOCs contribute substantially to SOA formation through gas-to-particle transformation processes (Atkinson et al., 2006). The regulation of VOCs emissions becomes crucial in simultaneously controlling fine particulate matter ($PM_{2.5}$) and O_3 pollution (Xu et al., 2016). Beyond their environmental impact, some VOCs pose health risks, including skin irritation and respiratory issues (Kampa and Castanas, 2008; Nuvolone et al., 2018). Therefore, quantifying VOCs concentration variations and identifying their sources is critical for a comprehensive understanding of their environmental and health effects.

The issue of VOCs pollution is particularly prominent in China, and VOCs are a key air pollutant subject to stringent control measures, especially in densely populated and highly developed urban areas. For instance, the Yangtze River Delta (YRD) in China, experiencing rapid economic development, has been frequently besieged by severe air pollution. VOCs, recognized as key precursors to SOA and O_3, have garnered increasing attention in this region (Li et al., 2019; Liu et al., 2022b; Zhan et al., 2021). Field observations conducted by An et al. (2014) revealed significant seasonal variations in VOCs concentrations in Nanjing, a representative city in the YRD region. Wang et al. (2020a) observed elevated levels of non-methane VOCs during colder seasons compared to warmer periods over the YRD region. Zhao et al. (2020) identified the highest average VOCs concentration during wintertime in Nanjing, presenting a critical potential for SOA formation during the frequent air pollution season. To effectively control VOCs pollution, a comprehensive understanding of its sources is imperative. VOCs sources can be classified into anthropogenic and natural emissions, with anthropogenic sources prevailing in urban atmospheres (Hui et al., 2020; Kelly et al., 2018; van der Werf et al., 2010). Shao et al. (2016) emphasized traffic emissions (34 %), industrial production (22 %), and solvent usage (18 %) as major anthropogenic sources of summer VOCs emissions in the YRD region. Concurrently, Xia et al. (2014) identified fuel combustion (28 %) and solvent usage (26 %) as primary sources of winter VOCs in Nanjing. Studies on the health effects of VOCs from different sources underscore the necessity for increased attention to sources such as petrochemical industries and solvent usage (Hsu et al., 2018; Zhang et al., 2021b; Zheng et al., 2020).

In response to escalating challenges posed by air pollution, China promulgated the "Action Plan for the Prevention and Control of Air Pollution" in 2013 and implemented the "Three-Year Action Plan for the Blue Sky" from 2018 to 2021 (Zheng et al., 2018; Zheng et al., 2021). Remarkably, concentrations of air pollutants derived from anthropogenic sources, including sulfur dioxide (SO_2), NO_x, carbon monoxide (CO), and $PM_{2.5}$, witnessed significant declines due to diverse industrial and energy structure adjustments (Zheng et al., 2018; Zheng et al., 2021). However, there is a notable gap in understanding the changes in ambient VOCs concentrations and sources under these clean air actions, limiting the assessment of the impact of such clean air actions on VOCs reduction.

This study addresses this gap by providing a quantitative analysis of ground-level observed winter VOCs concentrations in urban Nanjing between 2013 and 2021. Based on a machine learning approach, the anthropogenic and mereological drivers of changes in VOCs concentrations between the two years are identified and quantified. Meanwhile, the investigation includes changes in the O_3 formation potential (OFP) and SOA formation potential (SOAFP) between the two years. In addition, source apportionment of VOCs is conducted using the positive matrix factorization (PMF) model, offering insights into changes in ambient VOCs sources during the given periods. Finally, source-specific health risks of VOCs are characterized through statistical analysis.

2. Methods

2.1. Sampling site and instruments

The sampling site, located in the urban area of Nanjing (32°02′35″ N, 118°44′45″ E), typifies an urban environment in the YRD region, integrating commercial and residential zones. Essentially, this area harbors notable anthropogenic sources of VOCs, primarily stemming from vehicular emissions and solvent usage. Moreover, petrochemical and refining facilities are situated approximately 15–25 km to the north and south, respectively. This sampling site has been comprehensively described in previous studies (Zhang et al., 2017a; Zhang et al., 2017b).

On-line and continuous monitoring of VOCs was conducted using the TH-300B Atmospheric Volatile Organic Compounds Fast Online Continuous Automatic Monitoring System, an innovative creation by Wuhan Tianhong. The measurement periods extended from December 2013 to January 2014 and December 2021 to January 2022. The TH-300B monitoring system encompasses a carrier gas system, an electronic refrigeration ultra-low-temperature pre-concentration sampling system, a GC-FID/MS (Gas Chromatography-Flame Ionization Detector/Mass Spectrometry) analysis system, and a recording system. Throughout the monitoring process, ambient air samples were collected via the sampling system, traversed the pre-concentration system, and, under a frigid temperature of −150 °C, C2-C4 hydrocarbons in the atmosphere were captured by a PLOT column, while other VOCs were sequestered by a deactivated quartz capillary column. Subsequently, rapid heating was applied for compound resolution, guiding them into the analysis system. Following separation by the gas chromatography column, C2-C4 hydrocarbons were analyzed by the FID detector, and other VOCs were scrutinized by the MS detector. The entire process unfolded seamlessly through control software, integrating automated purging and calibration systems (Hui et al., 2019; Yang et al., 2019). Sampling intervals were established at 1 h. The detection limit range of the instrument is from 0.008×10^{-9} to 0.05×10^{-9}. A total of 79 volatile organic compounds were measured, including 29 alkanes, 10 alkenes, 1 alkyne, 23 halogenated hydrocarbons, and 16 aromatic hydrocarbons. Furthermore, complementary pollution data, encompassing hourly averages of CO, NO_2, $PM_{2.5}$, PM_{10}, and SO_2, were generously provided by the China Ministry of Ecology and Environment.

2.2. Random forest (RF) model

The RF algorithm, recognized for its robustness, combines multiple decision trees for classification and regression tasks, with each decision tree serving as a fundamental unit (Breiman, 2001). The RF can address regression problems by utilizing a set of decision trees that operate on binary recursive partitioning. The core concept involves randomly

sampling the initial dataset to generate multiple diverse data subsets. Each decision tree then extracts random samples from these data subsets and calculates results independently. Subsequently, the model aggregates the outputs from each decision tree to produce the final result. This methodology assesses the significance of each explanatory variable in elucidating the nonlinear impacts on the response variable. RF excels at handling high-dimensional data with numerous features, capturing both linear and nonlinear relationships among variables without requiring additional assumptions regarding independent or dependent variables. Compared to traditional statistical algorithms, the RF algorithm exhibits higher predictive accuracy and lower uncertainty for high-dimensional datasets, resulting in superior overall performance (Grange et al., 2018). The RF algorithm has been widely applied in the field of atmospheric environment (Lv et al., 2023; Shi et al., 2021). It is particularly effective in decoupling the impact of meteorological factors on air quality, thus providing a more accurate assessment of how air pollution responds to anthropogenic disturbances (Grange et al., 2018; Dai et al., 2021b; Vu et al., 2019; Zhou et al., 2022). In this study, we employed the RF model to quantify the contribution of anthropogenic emission control and meteorological variations on changes in VOCs concentrations between 2013 and 2021.

In this study, different air pollutant concentrations and 18 different meteorological conditions (Table S1) were input into the RF model. The model configuration includes a forest of 200 trees (n_tree = 200) and the number of variables that can be considered for splitting at each node (mtry = 3). More detailed parameters can be found in previous studies (Ji et al., 2023; Vu et al., 2019). In the RF modeling, 70 % of the entire dataset was partitioned as the training dataset, while the remaining 30 % was used for testing. Using the pollutant concentration and meteorological data from 2013 as a baseline for anthropogenic emission levels, an RF model will be established. This model will then be used to simulate pollutant concentrations in 2021 under the emission levels of 2013 and the meteorological conditions of 2021. By analyzing the difference between the observed and predicted concentrations, specific quantified results on the impact of anthropogenic emission reduction and meteorological conditions on air pollutants will be obtained.

$$\Delta_{obs(i,j)} = \Delta_{ant(i,j)} + \Delta_{met(i,j)} \tag{1}$$

$$\Delta_{met(i,j)} = C_{pred_j} - C_{pred_i} \tag{2}$$

$$\Delta_{ant(i,j)} = \Delta_{obs(i,j)} - \Delta_{met(i,j)} \tag{3}$$

Here, $\Delta_{obs(i,j)}$ represents the difference in observed concentrations between reference years i (e.g., 2013) and j (e.g., 2021) (Eq. (1)). $\Delta_{MET(i,j)}$ signifies the alterations attributed to meteorological variations during the same period, computed as the difference between the predicted concentrations in 2021 (C_{pred_j}) and in 2013 (C_{pred_i}) (Eq. (2)). $\Delta_{ant(i,j)}$ represent the changes between 2013 and 2021 resulting from anthropogenic emission control, calculated as the difference between $\Delta_{obs(i,j)}$ and $\Delta_{met(i,j)}$ (Eq. (3)).

To evaluate the performance of the RF model, multiple indicators are utilized in this study to assess the deviations between observed and predicted values. The main principle of the Eq. is as follows:

$$MAE = \frac{1}{n}\sum_{i=1}^{n}|x_i - y_i| \tag{4}$$

$$RMSE = \sqrt{\frac{\sum_{i=1}^{n}|x_i - y_i|}{n}} \tag{5}$$

$$NMSE = \frac{1}{n}\sum_{i=1}^{n}\frac{MSE}{VAR(x_i)} \tag{6}$$

$$R = \frac{\sum_{i=1}^{n}(x_i - \overline{x_i})(y_i - \overline{y_i})}{\sqrt{\sum_{i=1}^{n}(x_i - \overline{x_i})^2 \sum_{i=1}^{n}(y_i - \overline{y_i})^2}} \tag{7}$$

The Mean Absolute Error (*MAE*) represents the average of the absolute errors between Predicted (y_i) concentrations in the test dataset and observed (x_i) concentrations (Eq. (4)). The Root Mean Square Error (*RMSE*) is derived as the square root of the average of the squared differences between predicted and observed concentrations (Eq. (5)), normalized by the square root of the number of observations, indicating the spread of the predictions. The Normalized Mean Squared Error (*NMSE*) enhances the mean squared error by standardizing it (Eq. (6)); a lower ratio suggests that the model outperforms a strategy based solely on predicting with the mean. The Pearson correlation coefficient R signifies the linear correlation between two variables (Eq. (7)), $\overline{x_i}$ and $\overline{y_i}$ respectively represent the averages of observed values and predicted values. When their values are close to 1, it indicates an excellent correlation between them. Notably, the observed concentrations of each pollutant exhibit a high correlation with the model's predicted concentrations (Fig. S1). MAE (0.18–29.21), RMSE (0.25–42.06), NMSE (0.18–0.37), all correlation coefficients exceeding 0.8. These results demonstrate the robustness and reliability of the RF model established in this study.

2.3. Source apportionment with PMF

In this study, the PMF model (Paatero and Tapper, 1994) was employed to decompose the total VOCs into several sources. The PMF model decomposes the sample data matrix into a factor contribution matrix and a factor spectrum matrix, identifies the factor spectrum matrix, and quantitatively calculates the sample's factor contribution. The principle is elucidated by the following equation:

$$x_{ij} = \sum_{k=1}^{p} g_{ik} f_{kj} + e_{ij} \tag{8}$$

Here, x_{ij} represents the concentration of the jth species measured in the ith sample (Eq. (8)); g_{ik} is the contribution of the kth source to the ith sample; f_{kj} is the jth component of the kth source; and e_{ij} is the residual for each species (Paatero, 1997). In the specific calculation, the uncertainty of VOCs is first computed, directly affecting the input mass concentrations and component concentrations of VOCs in the PMF model. The calculation weight of the data is determined based on the following Eqs.:

$$unc = \frac{5}{6} \times MDL \tag{9}$$

$$unc = \sqrt{(EF \times Conc)^2 + (0.5 \times MDL)^2} \tag{10}$$

Here, *unc* is the uncertainty of VOCs components (ppb); *MDL* is the detection limit of particle analysis components, primarily determined by the sensitivity of the monitoring instrument; *Conc* is the mass concentration of VOCs components (ppb); *EF* (Error fraction) is the error coefficient of particle analysis components, referring to the instrument's RSD value, set to 0.1. When *Conc* is less than or equal to *MDL*, (Eq. (9)) is used for calculation. When *Conc* is greater than *MDL*, (Eq. (10)) is applied. During computation, the model categorizes data into three classes based on the signal-to-noise ratio (S/N) of the input data, dividing them into "bad," "weak," and "strong" categories. Data points with (S/N < 0.2) are classified as "bad" and discarded. Data with (0.2 < S/N < 2) are considered "weak," and their corresponding uncertainty is tripled for weighting. Data with (S/N > 2) are regarded as "strong" and directly used for PMF analysis. The software US EPA PMF 5.0 was used to achieve the PMF calculation in this study (Norris et al., 2014).

In this study, a total of 36 VOCs were input into the PMF model for

source apportionment, including 21 alkanes, 6 alkenes, 9 aromatic compounds, and acetylene (Table S2). The selection criteria were based on having high mixing ratios and low uncertainties common in 2013 and 2021, representativeness in sources, or suitability as tracers. As shown in Fig. S2, the number of factors was set between 4 and 8. As the number of factors increased, the trend of decreasing Q_{true}/Q_{robust} ratio became evident. The variation in the Q_{true}/Q_{robust} values during the three years decreased as the number of factors increased to 7, indicating that this number of factors was adequate (Yang et al., 2023). The factor operation underwent 100 bootstrapping analyses to reduce errors and enhance the accuracy of the results. The rationality of the percentage contribution of each factor source in different years was analyzed, ultimately confirming the 6-factor solution.

2.4. Calculation of OFP and SOAFP

Numerous studies on O_3 formation mechanisms have proposed various methods for quantifying the generation of O_3 from VOCs (Kleinman, 2000; Lin et al., 2009). Currently, widely used simplified methods are as follows:

$$OFP_i = [VOC_i] \times MIR_i \tag{11}$$

In Eq. (11), OFP_i represents the Ozone Formation Potential of VOCs (μg/m^3); VOC_i is the mass concentration of VOCs (μg/m^3); and MIR_i is the Maximum Incremental Reactivity of VOCs. Similarly, secondary aerosol formation potential (SOAFP) quantifies the ability of VOCs to form secondary organic aerosols (Liu et al., 2022a), and its Eq. is expressed as:

$$SOAFP_i = [VOC_i] \times SOAP_i \tag{12}$$

where $SOAFP_i$ in Eq. (12) is the SOA Formation Potential of VOCs (μg/m^3), and $SOAP_i$ is the coefficient representing the formation of SOA by VOCs.

2.5. Health risk assessment

In this study, quantitative health risk assessment of the monitored VOCs was conducted using the method of the United States Environmental Protection Agency (US EPA), in order to investigate the impact of different types and sources of VOCs on human health. The following are the relevant calculation Eqs.:

$$EC = \frac{(CA \times ET \times EF \times ED)}{AT} \tag{13}$$

$$LCR = IUR \times EC \tag{14}$$

In Eq. (13), EC represents the exposure concentration (μg/m^3); CA is the environmental concentration (μg/m^3); ET is the exposure time (hours/day); EF is the exposure frequency (days/year); ED is the exposure duration (years); and AT is the averaging time (hours). In this study, EF is set to 365 days/year, ET is 3.7 h/day, and ED is 74.8 years. In Eq. (14), LCR stands for lifetime carcinogenic risk (μg/m^3); IUR is the inhalation unit risk; The IUR values for different species are obtained from the Risk Assessment Information System (RAIS).

2.6. Concentration-weighted trajectories (CWT)

In this study, we employed the Hybrid Single-Particle Lagrangian Integrated Trajectory (HYSPLIT) model (Draxler and Rolph, 2014) to calculate 48-h backward trajectories at a height of 100 m above ground level, with 3-h intervals, using data from the Global Data Assimilation System (GDAS). By integrating these trajectories with CWT analysis, we simulated various temporal and source trajectories of VOCs to identify the patterns of VOCs originating from different atmospheric sources. The geographical resolution for these calculations is 0.25° × 0.25°. The CWT method assigns weights to trajectories based on pollutant concentrations, with CWT values indicating the likelihood of pollution trajectories in specific areas (Petit et al., 2017). The CWT value calculation in this study was performed using an Igor-based toolkit (ZeFir) developed by Petit et al. (2017).

3. Results and discussion

3.1. Drivers of changes in VOCs concentrations between 2013 and 2021

The concentrations of major air pollutants have exhibited varying degrees of decrease from 2013 to 2021, as depicted in Fig. S3. Particularly noteworthy is the substantial decrease in SO_2 (72.8 %), followed by $PM_{2.5}$ and PM_{10}, with reductions of 59.2 % and 53.3 % respectively. CO and NO_2 experienced decreases of 37.3 % and 39.2 % respectively. Anthropogenic emissions have primarily driven the decrease in concentration of each air pollutant (>84 %), underscoring the effectiveness of China's emission reduction policies in the Nanjing region since 2013.

Fig. 1 illustrates the concentration changes in various VOCs between 2013 and 2021, driven by both anthropogenic emissions and meteorological conditions. In 2021, the average mixing ratio of total VOCs (TVOCs) was 33.9 ± 21.6 ppb, corresponding to a 35.3 % decrease compared to the 2013 value of 52.4 ± 30.4 ppb. The concentration driven by anthropogenic emissions is 17.4 ± 21.5 ppb, accounting for 94.3 % of the total decrease. Compared to the average mixing ratio in other cities in 2021, the results indicate that it is higher than Beijing (Liang et al., 2023) (17.4 ± 10.1 ppbv), close to Guangzhou (Zou et al., 2023) (32.3 ppbv), and lower than Kaifeng (Chen et al., 2023) (43.2 ppb). The different VOC categories, with substantial declining ratios obtained, by order of importance, for alkenes (52.7 %), halocarbons (41.9 %), alkanes (34.2 %), acetylene (29.3 %), and aromatics (24.5 %). The concentration changes driven by anthropogenic emissions contributed to 4.4 ± 3.4, 1.3 ± 2.7, 8.7 ± 11.9, 1.2 ± 2.6, and 1.6 ± 5.0 ppb, respectively.

Alkanes exhibited the highest mixing ratio and relative contribution in both 2013 (27.2 ± 18.1 ppb, 52 %) and 2021 (18.2 ± 11.8 ppb, 54 %), respectively (Fig. S4). Fig. S5 presents the average mixing ratios of individual VOCs in 2013 and 2021, revealing substantial reductions for higher-chain alkanes in 2021. Alkenes, primarily associated with petrochemical and vehicle exhaust emissions, experienced a notable decrease (8.1 ± 5.3 ppb, 11.0 %) compared to 2013 (3.9 ± 2.8 ppb, 15 %). Acetylene, halocarbons, and aromatics exhibited slightly higher contributions in 2021 (9.1 %, 10.2 %, and 16.0 %) compared to 2013 (7.8 %, 8.6 %, and 13.0 %), respectively. Previous studies have suggested that acetylene and certain halocarbons serve as tracers for combustion processes, while aromatic compounds often originate from solvent usage (Liu et al., 2008; Zhang et al., 2009; Hui et al., 2018; Wang et al., 2013). The differences in chemical composition between the two years may be attributed to the variations in the sources of VOCs.

3.2. Contributions of VOCs to OFP and SOAFP

VOCs serve as critical precursors for O_3 and SOA formation. Even identical compounds can have varying effects on the formation of ozone and SOA due to undergoing different reactions and producing diverse intermediate products in the atmosphere under varied meteorological conditions (Li et al., 2020). A meticulous comparison of the species and concentrations of OFP and SOAFP between 2013 and 2021 is imperative for a nuanced understanding of VOCs and the implementation of effective control measures.

In 2013, the total OFP concentration was 332.3 ± 241.0 μg/m^3, experiencing a notable decrease of approximately 32.1 % to 225.6 ± 195.4 μg/m^3 by 2021. When compared to other cities, winter OFP levels in Nanjing are observed to be lower than those in Rizhao (504.6 μg/m^3) (Zhang et al., 2023), yet higher than those reported for Beijing (102 μg/m^3) (Liang et al., 2023) and Taiyuan (93.40 ppb) (Wang et al., 2023b).

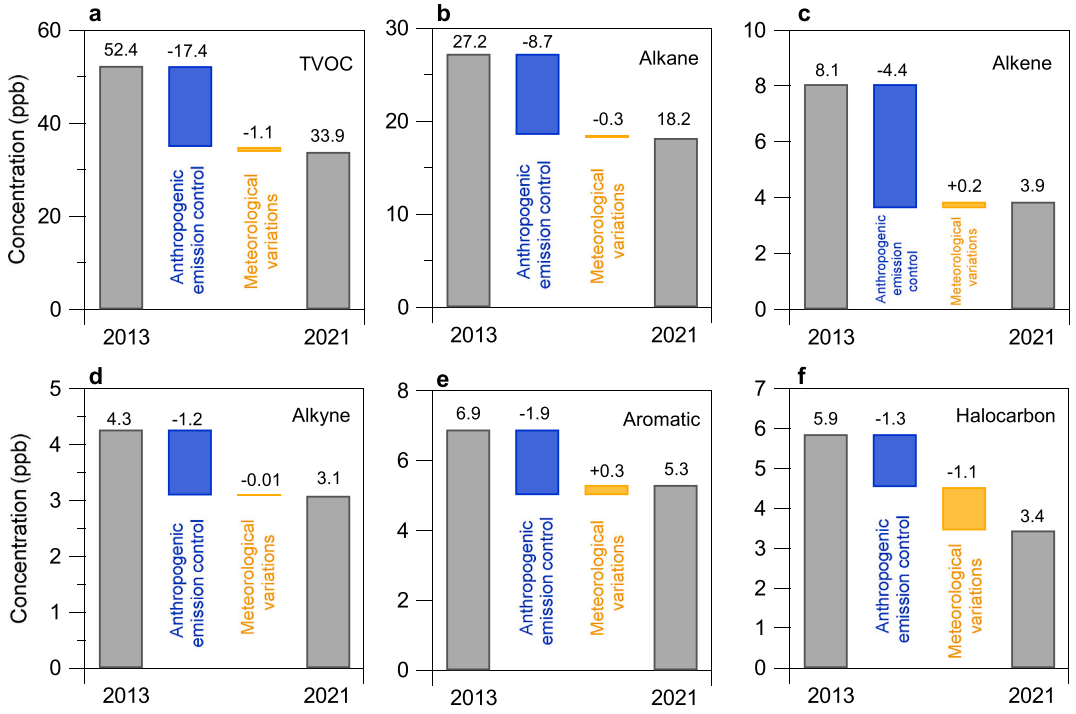

Fig. 1. The changes in average VOCs concentrations during wintertime between 2013 and 2021 driven by anthropogenic emission control and meteorological variations, respectively.

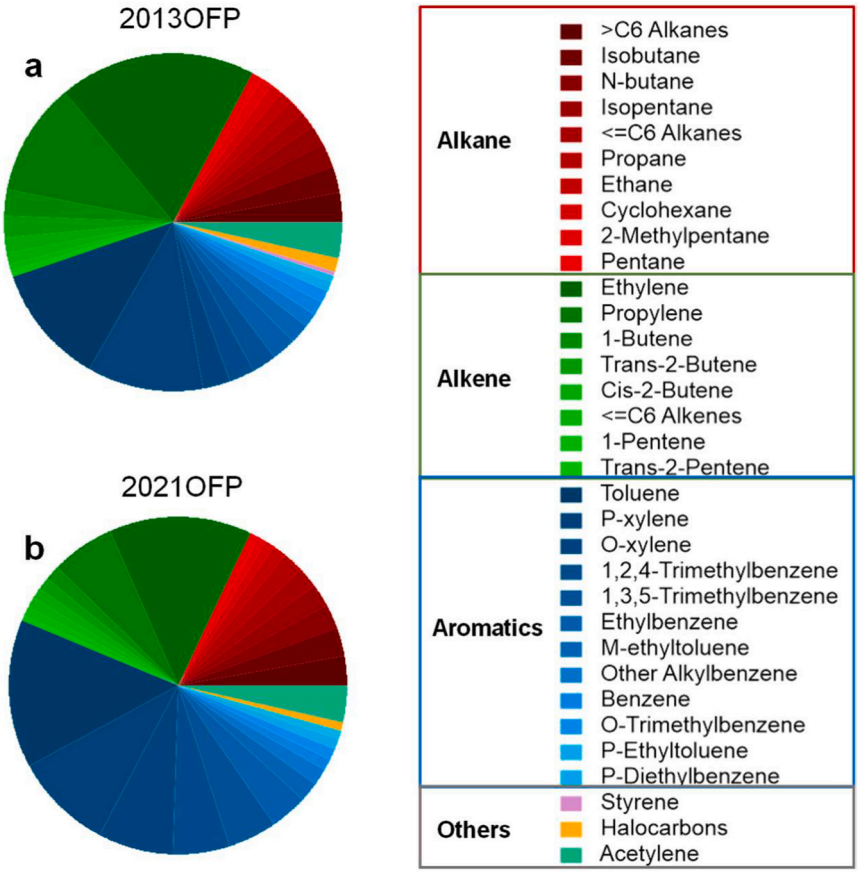

Fig. 2. Relative contribution of various VOCs to OFP during wintertime in 2013 (a) and 2021 (b), respectively.

Among the various VOC categories, alkenes exhibited the most substantial reduction in contribution (53.9 %), followed by alkanes (29.4 %), acetylene (29.3 %), and aromatics (11.9 %). Fig. 2 visually represents the relative contributions of each VOC category to OFP in 2013 and 2021, consistently ranking aromatics, alkenes, alkanes, acetylene, and halocarbons from highest to lowest in both years. These findings are consistent with prior studies (Lv et al., 2021; Song et al., 2021). Additionally, Fig. S6 provides further insights by delineating the top ten dominant species contributing to OFP in both 2013 and 2021, showcasing a diverse array of alkenes and aromatics.

The total SOAFP concentrations were 137.1 ± 125.5 μg/m^3 in 2013 and 99.6 ± 101.5 μg/m^3 in 2021, signifying a reduction of approximately 27.4 %. As depicted in Fig. 3, the wide majority of SOAFP originated from aromatic compounds, accounting for 96.1 % in 2013 and 96.9 % in 2021. These results are consistent with research findings in other cities in eastern China (Wang et al., 2023a; Zhang et al., 2021a). Fig. S7 elucidates the top ten species contributing to SOAFP in 2013 and 2021, with toluene consistently holding the highest contribution in both years, at 54.4 μg/m^3 in 2013 and 30.5 μg/m^3 in 2021, reflecting a 44.0 % reduction. The findings underscore the pivotal role of controlling aromatic and alkenes emissions for enhancing air quality concerning O_3 and SOA pollution.

3.3. Source analysis of VOCs

Fig. 4 presents the PMF resolved profiles of six factors for both 2013 and 2021. In 2013, factors are denoted from a to f, while factors for 2021 are labeled from g to l. Factor a in 2013 and factor g in 2021 both exhibited significant contributions from aromatic compounds. Specifically, factor a (Fig. 4a) contributed 66.6 %, 55.8 %, 57.5 %, and 54.9 % to ethylbenzene, toluene, m/p-xylene, and o-xylene, respectively. Similarly, factor g (Fig. 4g) contributed 61.5 %, 52.4 %, 30.5 %, and 23.1 % to o-xylene, 1-ethyl-3-methylbenzene, p-xylene, and ethylbenzene, respectively. These factors have been identified as sources associated with paint and solvent usage, emitting substantial quantities of C7–C9 aromatic hydrocarbons (Yuan et al., 2010; Zheng et al., 2013).

In 2013, ethane, propane, and ethylene showed relatively high mass percentages (Fig. 4b) in factor b (32.9 %, 14.6 %, 10.3 %). Additionally, factor b had significant contributions to pentene and isoprene, with percentages of 84.9 % and 31.0 %, respectively. Pentene is a raw material for the production of isoprene and can be obtained through the pyrolysis fractionation of petroleum (Guo et al., 2004). In addition to its wide application in the chemical industry, isoprene is largely emitted from plants (Lau et al., 2010), but the effect of plants is not significant in winter. Therefore, Factor b is identified as being associated with the petrochemical source of pentene. In 2021, factor h (Fig. 4h) contributed significantly to ethylbenzene and styrene, both crucial materials in the production of styrene, an essential component in the petrochemical industry (Li et al., 2017b). Thus, factor h is identified as being associated with the petrochemical source of ethylbenzene. Both factors b and h are indeed identified as petrochemical sources, yet they exhibit distinct characteristics. This disparity can be attributed to two possible factors. Firstly, the petrochemical industry encompasses a diverse array of materials and emissions, resulting in a wide variety of VOC types. Secondly, adjustments in the petrochemical industry structure between 2013 and 2021 have led to changes in the types of VOCs produced, contributing to the observed differences between the two factors.

Factor c (Fig. 4c) in 2013 had high contributions to benzene, trimethylpentane, methylcyclohexane, and methylcyclopentane, with percentages of 50.8 %, 61.0 %, 50.8 %, and 48.2 %, respectively. Benzene, a common chemical raw material, showed the highest mass percentage in factor c (20.2 %). Methylcyclopentane and methylcyclohexane are common industrial products. The strong correlation between benzene and methylcyclohexane ($r = 0.63$) and benzene and methylcyclopentane ($r = 0.59$) (Fig. S8a, b) led to the identification of factor c as an industrial source related to benzene. In 2021, factor i (Fig. 4i) displayed a high mass percentage of toluene (45.9 %) and contributed 61.1 % to toluene. Toluene has widespread industrial applications and serves as a significant precursor for various products, including rubber, explosives, and dye intermediates (Filley et al., 2004). Factor i was identified as an industrial source related to toluene.

In 2013, factor d (Fig. 4d), and in 2021, factor j (Fig. 4j), were composed of high mass percentages of ethane, propane, ethylene, and acetylene (13.8 %–32.9 % for factor d, and 8.7 %–26.0 % for factor j). These compounds are typical products of coal and biomass combustion (Sun et al., 2018). Factors d and j exhibited a strong correlation with CO ($r = 0.56$ and $r = 0.50$, respectively) (Fig. S8c and d) and were identified as sources related to solid fuel combustion.

Factors e (Fig. 4e) and k (Fig. 4k) were defined as sources related to liquefied petroleum gas (LPG) and natural gas (NG). Both factors exhibited high mass percentages of ethane, propane, and butane (8.0 %–20.7 % for factor e, and 5.3 %–20.9 % for factor k). Unlike fossil fuel and biomass combustion sources, these factors had higher contributions to butane, with percentages of 23.8 % and 36.5 %, respectively. These substances often originate from LPG, NG, and their combustion products (Ho et al., 2009).

C4–C5 alkanes and alkenes, such as n-pentane, isopentane, 1-butene, and 2-butene, are major components of automobile exhaust emissions (Li et al., 2017a; Zhang et al., 2013). In 2013, factor f (Fig. 4f), and in 2021, factor l (Fig. 4l), contributed 29.0 %–83.2 % and 43.8 %–98.2 %, respectively, to these compounds. Methyl tert-butyl ether (MTBE), a typical tracer for automobile exhaust emissions (Chang et al., 2003), exhibited a strong correlation with factors f and l ($r = 0.53$ and $r = 0.62$, respectively) (Fig. S8e, f). Vehicle exhaust emissions generate a large amount of nitrogen oxides. Correlation analyses between NO_2 and factors f, l showed a good correlation, with $r = 0.70$ and $r = 0.62$, respectively (Fig. S8g and h). Therefore, these two factors were named as sources related to vehicle emission.

Fig. S9 depicts the diurnal variations of VOCs from different sources in 2013 and 2021, respectively. Most sources exhibit lower levels during the daytime and higher levels in the early morning and evening. This pattern can be attributed to two factors. Firstly, strong solar radiation

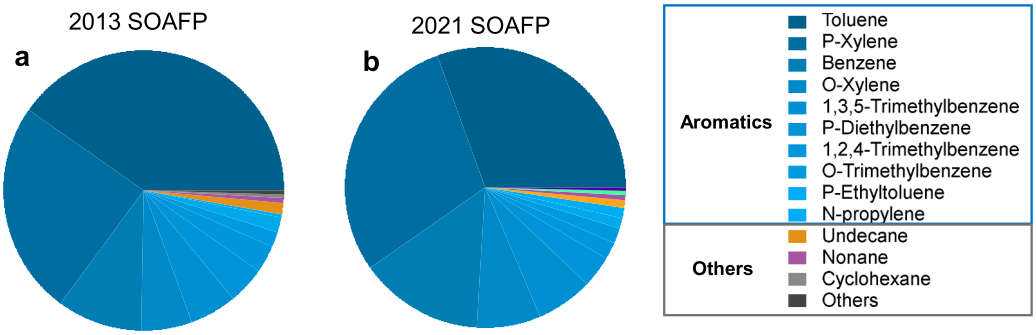

Fig. 3. Relative contribution of various VOCs to SOAFP during wintertime in 2013 (a) and 2021 (b), respectively.

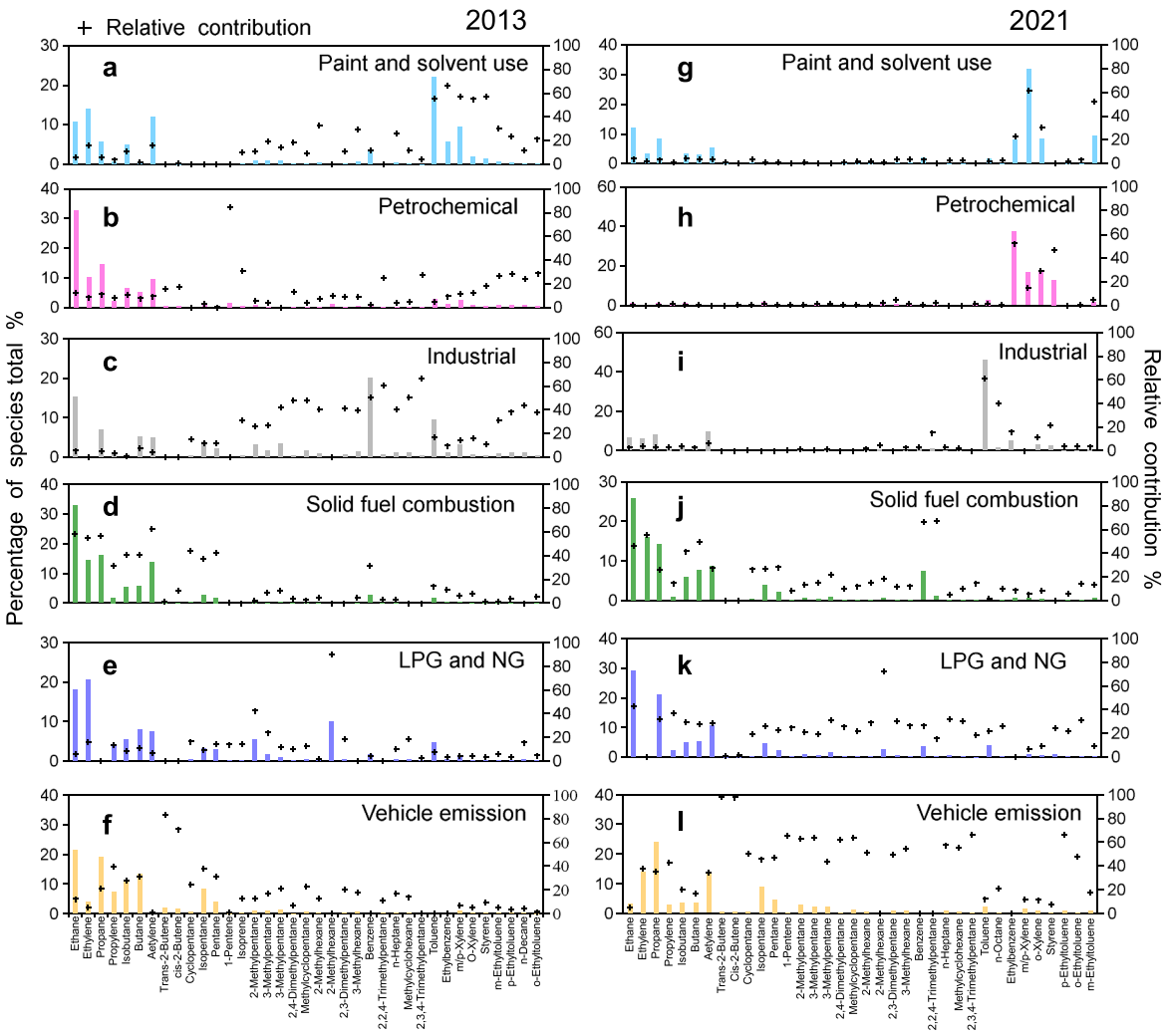

Fig. 4. PMF-resolved factor profiles for six VOCs sources during wintertime in 2013 (a–f) and 2021 (g–l), respectively.

during the day leads to a higher atmospheric boundary layer, resulting in a certain degree of VOCs dilution (Yang et al., 2012). Secondly, intense solar radiation increases the photochemical reaction rate of VOCs (Zhang et al., 2016), leading to generally lower VOCs concentrations during the day. Interestingly, similar diurnal variation characteristics are observed for the same sources across different years. For instance, the source of paint and solvents use is mainly composed of aromatic compounds (Fig. S9a) exhibits weaker photochemical reactions during the day due to the relatively stable chemical properties of benzene rings. The vehicle emissions source (Fig. S9f) shows noticeable concentration spikes during the morning rush hour (7–9 am) and evening rush hour (5–7 pm), aligning with the commuting patterns of individuals.

Fig. 5 illustrates the composition and relative contribution of VOCs from different sources during the winter seasons of 2013 and 2021, respectively. In 2013, the top three contributors were solid fuel combustion (16.1 ppb, 43.6 %), followed by vehicle emission (5.2 ppb, 16.7 %), and paint and solvent use (4.7 ppb, 12.8 %). By 2021, the leading sources had shifted, with solid fuel combustion (8.7 ppb, 31.9 %), liquefied petroleum gas and natural gas (7.3 ppb, 26.8 %), and vehicle emission (6.9 ppb, 25.5 %). Comparing the two years, there have been noticeable decreases in the contributions of paint and solvent use, petrochemical, industry, and solid fuel combustion, as depicted in Figs. S10a–d. Vehicle emission source remained relatively stable during this period. The decline in solid fuel combustion (45.9 %) indicates the success of stricter regulations on biomass and coal burning, while the

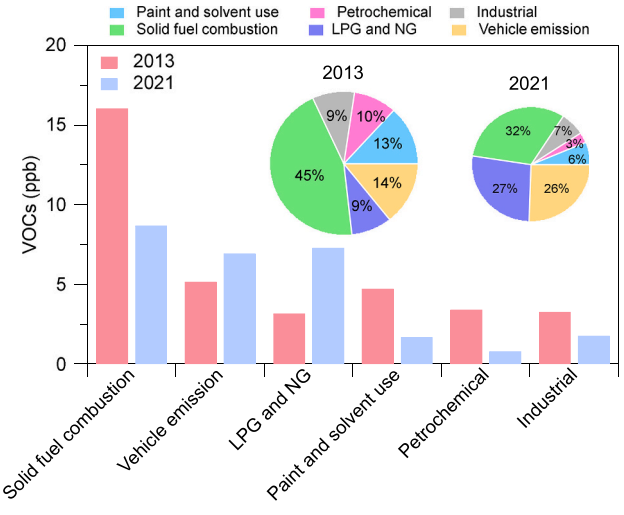

Fig. 5. Concentration and relative contribution of VOCs sources during wintertime in 2013 and 2021, respectively.

rise in liquefied petroleum gas and natural gas usage (129.4 %) reflects China's increased consumption and proportion of natural gas in its energy mix. According to the "China Natural Gas Development Report",

China's natural gas consumption increased from 167.6 billion cubic meters in 2013 to 369.0 billion cubic meters in 2021, with its share in primary energy consumption rising from 5.9 % to 8.9 % (Dai et al., 2021a; Li, 2022). These findings demonstrate significant progress in optimizing China's energy structure between 2013 and 2021, potentially influencing the distribution of VOCs sources in the YRD region.

In addition to emissions, the influence of regional transport is a crucial factor to consider in studying VOC pollution (Fan et al., 2021; Wang et al., 2022). The average winter surface wind speeds in Nanjing were 2.73 m/s in 2013 and 2.70 m/s in 2021, respectively. Referring to the VOCs pollution rose diagram (Fig. S11), it can be noted that VOCs were primarily influenced by winds from the northeast and east directions in both 2013 and 2021. Furthermore, we categorized all air masses in 2013 into six clusters and five clusters in 2021 (Fig. 6). Notably, the trajectories and contribution percentages of clusters 2–6 in 2013 correspond to clusters 1–5 in 2021. Clusters 2 and 5 in 2013 primarily represent long-distance transport from the northwest and north, corresponding to clusters 1 and 5 in 2021. These clusters exhibit longer trajectories and lower VOC mixing ratios, accounting for 6.4 % and 18.7 % in 2023 and 3.3 % and 12.5 % in 2021, respectively. A longer transport pathway indicates that air masses have relatively faster movement speeds and shorter residence times in the atmosphere (Liu et al., 2021; Niu et al., 2022), which suggests that sources such as solid fuel combustion, C2-C4 alkanes and alkenes, LPG, and NG have a higher proportion in these clusters. In this study, ethane (16.3 %–28.2 %) and propane (13.6 %–22.8 %) emerge as the primary contributing species associated with these clusters. Clusters 3 and 4 in 2013 correspond to clusters 3 and 2 in 2021, originating from the northeast and northwest, respectively, with VOC sources displaying a relatively uniform distribution. Ethane (15.4 %–18.3 %) and propene (7.6 %–12.1 %) are among the primary contributing species. Cluster 6 in 2013 corresponds to cluster 4 in 2021, originating from short-distance transport from the north. With the mixing ratios of this cluster being the highest in both years, accounting for 32.3 % and 36.7 %. The findings are also in line with the horizontal transport of VOCs close to the ground. A shorter transport pathway indicates slower movement of air masses, facilitating the accumulation of VOCs during short-distance transport processes (Liu et al., 2024). This phenomenon may be associated with stable weather conditions. In these clusters, solid fuel combustion, LPG, and NG remain dominant sources, comprising 31.2 %, 21.3 % in 2013, and 26.2 %, 32.5 % in 2021. The proportion of vehicle emissions has increased from 12.4 % to 26.2 %. Ethylene (13.2 %–20.6 %) and butane (11.1 %–22.0 %) made substantial contributions to the total VOCs associated with these clusters. These research findings are consistent with those of Niu et al. (2022), who reported similar observations during the heating period in Beijing. They found that primary coal combustion (30.9 %), vehicular exhaust (27.7 %), and LPG/NG (17.5 %) were the primary contributors associated with short-distance transport.

3.4. Source-specific health risk assessment of VOCs

In addition to their impact on the atmospheric environment, certain VOCs exhibit toxicity, posing potential health risks to humans. This study addresses the LCR of 11 selected VOCs for the years 2013 and 2021. The acceptable safety threshold level and the tolerable safety threshold level for LCR are 1×10^{-6} and 1×10^{-4}, respectively (US EPA). Fig. 7 illustrates the dominant species contributing to LCR, predominantly halogenated hydrocarbons and aromatic hydrocarbons. The total LCR value in 2021 $(2.2 \pm 1.3) \times 10^{-5}$ marked a 72.6 % reduction compared to 2013 $(8.2 \pm 6.6) \times 10^{-5}$. While seven VOCs exceeded the acceptable threshold in 2013, this number decreased to six in 2021. The LCR values for various VOCs have not exceeded the tolerable threshold in either year. Species with consistently higher LCR in both years include dibromoethane, benzene, and carbon tetrachloride. Notably, in 2021, their LCR values (9.0×10^{-6}, 6.5×10^{-6}, 2.3×10^{-6}) decreased by 83.2 %, 44.1 %, and 57.6 %, respectively, compared to 2013 (5.4×10^{-5}, 1.2×10^{-5}, 5.4×10^{-6}). Despite the significant reduction in LCR of VOCs from 2013 to 2021, certain species (dibromoethane, benzene, carbon tetrachloride, ethylbenzene, 1,2-dichloroethane, trichloroethylene) still surpass the safety threshold. Similar to results from Zhengzhou (Zhang et al., 2021c), chloroform, 1,2-dichloroethane, and 1,2-dibromoethane are the main species that exceed the acceptable threshold.

Additionally, utilizing the 6-factor PMF results for 2013 and 2021, we estimated the relative contributions of each pollution source to LCR through the "source risk allocation" point estimate method, applied in other studies (Bari and Kindzierski, 2018; Wang et al., 2009; Zhang et al., 2021b). Fig. 8 reveals that in 2013, the LPG and NG sources accounted for the majority of LCR (49.9 %), decreasing to 29.0 % in 2021. However, it, along with the vehicle emission source (29.4 %), continues to be a significant contributor to LCR. The contribution of solid fuel and biomass combustion, as well as industrial sources to the LCR, increased in 2021 to 18.6 % and 14.6 %, respectively, compared to 8.9 % and 8.6 % in 2013. Conversely, the contributions from petrochemical sources and the use of paint and solvents decreased to 1.5 % and 6.7 % in 2021, down from 11.7 % and 11.4 % in 2013, respectively. Consequently, targeted reduction of emissions from prevalent VOCs and

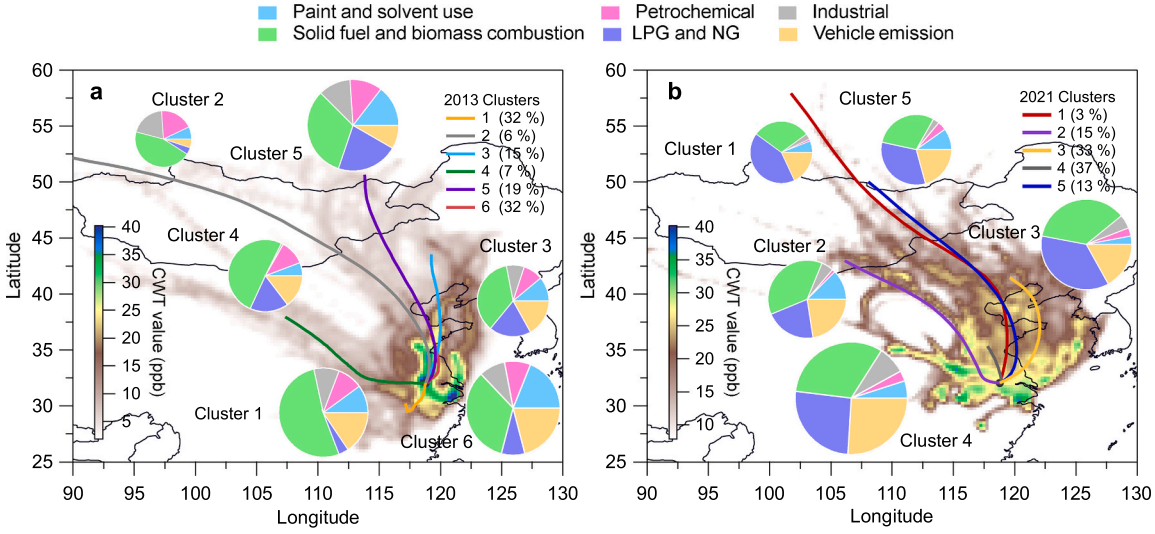

Fig. 6. The CWT analysis along with different air mass clusters corresponding to relative contribution of VOCs sources during wintertime in 2013 (a) and 2021 (b), respectively.

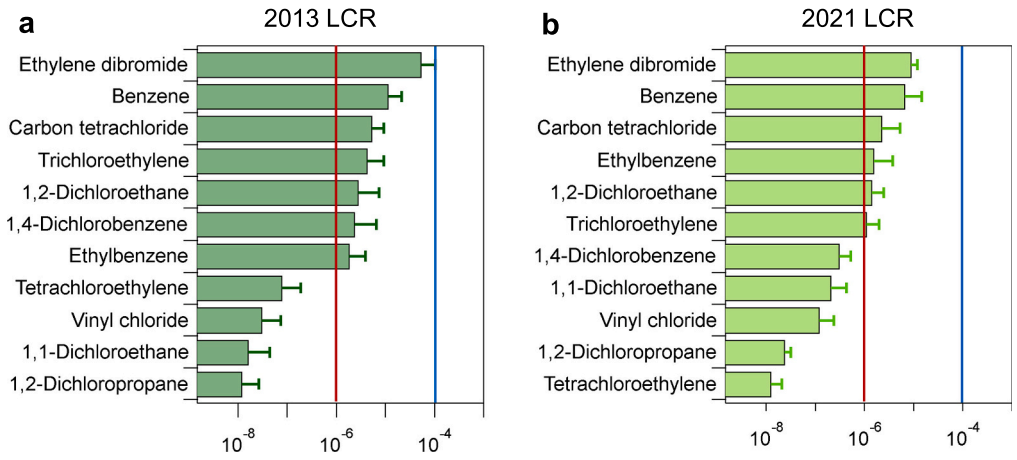

Fig. 7. Lifetime carcinogenic risk (LCR) value for the major VOCs species during wintertime in 2013 (a) and 2021 (b), respectively.

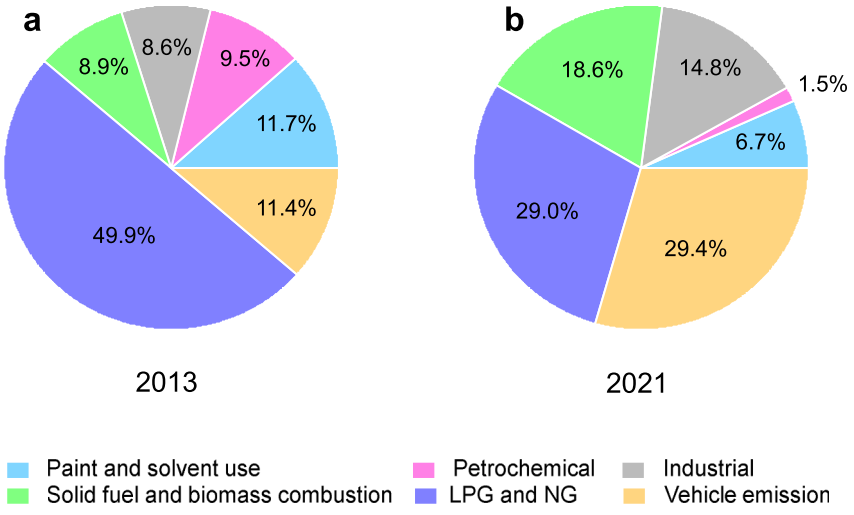

Fig. 8. Relative contribution of VOCs sources to the LCR during wintertime in 2013 (a) and 2021 (b), respectively.

their associated sources is imperative to mitigate their impact on human health.

4. Conclusion

This study, focusing on atmospheric VOCs in urban Nanjing during the winters of 2013 and 2021, reveals a significant decrease in total VOCs concentration from 52.4 ± 30.4 ppb to 33.9 ± 21.6 ppb. By employing the machine learning method, we quantified the impact of anthropogenic emissions and meteorological variations on VOCs. Our findings underscore anthropogenic emissions as the primary driving factor, with VOCs categories ranked in descending order of decline ratios: alkenes (51.9 %), halogenated hydrocarbons (42.4 %), alkanes (33.1 %), acetylene (27.9 %), and aromatic hydrocarbons (23.2 %). The OFP value decreased by approximately 32.1 %, while the SOAFP value decreased by approximately 27.4 %. Utilizing the PMF model, we identified six distinct VOCs sources. In 2013, primary contributors were solid fuel combustion (43.6 %), vehicle emissions (16.7 %), and paint and solvent use (12.8 %). By 2021, major sources shifted to solid fuel combustion (31.9 %), liquefied petroleum gas and natural gas (26.8 %), and vehicle emissions (25.5 %). Notably, solid fuel combustion decreased significantly (45.9 %), aligning with China's energy structure adjustments. Health risk assessment reveals a commendable 72.6 % decrease in the LCR in 2021 compared to 2013. Despite improvements, some species (such as dibromoethane, benzene, and carbon tetrachloride) still exceed acceptable LCR thresholds. Source risk allocation analysis attributes the majority of LCR to liquefied petroleum gas and natural gas sources, as well as vehicle emission sources in both years, highlighting the need for targeted emissions reduction from these sources to minimize health risks.

CRediT authorship contribution statement

Zihang Zhang: Data curation, Formal analysis, Methodology, Software, Visualization, Writing – original draft. **Yunjiang Zhang:** Conceptualization, Funding acquisition, Methodology, Software, Supervision, Writing – review & editing. **Sheng Zhong:** Data curation, Formal analysis, Writing – review & editing. **Jie Fang:** Formal analysis, Software, Visualization. **Baoru Bai:** Writing – review & editing. **Cheng Huang:** Conceptualization, Supervision, Writing – review & editing. **Xinlei Ge:** Writing – review & editing.

Declaration of competing interest

The authors declare that they have no known competing financial interests or personal relationships that could have appeared to influence the work reported in this paper.

Data availability

Data will be made available on request.

Acknowledgements

This study was supported by Natural Science Foundation of Jiangsu Province (grant no. BK20210663) and the Natural Science Foundation of China (grant no. 42207124). The authors acknowledge Dr. Valérie Gros (Laboratoire des Sciences du Climat et de l'Environnement, CNRS-CEA-UVSQ, Université Paris-Saclay, France), and Dr. Olivier Favez (Institut National de l'Environnement Industriel et des Risques, France) for their insightful and helpful inputs.

Appendix A. Supplementary data

Supplementary data to this article can be found online at https://doi.org/10.1016/j.scitotenv.2024.173713.

References

An, J., Zhu, B., Wang, H., Li, Y., Lin, X., Yang, H., 2014. Characteristics and source apportionment of VOCs measured in an industrial area of Nanjing, Yangtze River Delta, China. Atmos. Environ. 97, 206–214.
Atkinson, R., 2000. Atmospheric chemistry of VOCs and NOx. Atmos. Environ. 34, 2063–2101.
Atkinson, R., 2007. Gas-phase tropospheric chemistry of organic compounds: a review. Atmos. Environ. 41, 200–240.
Atkinson, R., Baulch, D.L., Cox, R.A., Crowley, J.N., Hampson, R.F., Hynes, R.G., Jenkin, M.E., Rossi, M.J., Troe, J., Subcommittee, I., 2006. Evaluated kinetic and photochemical data for atmospheric chemistry: volume II – gas phase reactions of organic species. Atmos. Chem. Phys. 6, 3625–4055.
Bari, M.A., Kindzierski, W.B., 2018. Ambient volatile organic compounds (VOCs) in Calgary, Alberta: sources and screening health risk assessment. Sci. Total Environ. 631-632, 627–640.
Breiman, L., 2001. Random forests. Mach. Learn. 45, 5–32.
Chang, C.-C., Lo, S.-J., Lo, J.-G., Wang, J.-L., 2003. Analysis of methyl tert-butyl ether in the atmosphere and implications as an exclusive indicator of automobile exhaust. Atmos. Environ. 37, 4747–4755.
Chen, Y., Shi, Y., Ren, J., You, G., Zheng, X., Liang, Y., Simayi, M., Hao, Y., Xie, S., 2023. VOC species controlling O3 formation in ambient air and their sources in Kaifeng, China. Environ. Sci. Pollut. Res. 30, 75439–75453.
Dai, J., Ni, Y., Dong, D., Qin, S., Zhu, G., Huang, S., Yu, C., Gong, D., Hong, F., Zhang, Y., Yan, Z., Liu, Q., Wu, X., Feng, Z., 2021a. 2021–2025 is a period of great development of China's natural gas industry: suggestions on the exploration and development of natural gas during the 14th five-year plan in China. J. Nat. Gas. Geosci. 6, 183–197.
Dai, Q., Hou, L., Liu, B., Zhang, Y., Song, C., Shi, Z., Hopke, P.K., Feng, Y.J.G.R.L., 2021b. Spring Festival and COVID-19 lockdown: disentangling PM sources in major Chinese cities. Geophys. Res. Lett. 48, e2021GL093403.
de Gouw, J.A., Middlebrook, A.M., Warneke, C., Goldan, P.D., Kuster, W.C., Roberts, J. M., Fehsenfeld, F.C., Worsnop, D.R., Canagaratna, M.R., Pszenny, A.A.P., Keene, W. C., Marchewka, M., Bertman, S.B., Bates, T.S., 2005. Budget of organic carbon in a polluted atmosphere: results from the New England Air Quality Study in 2002. J. Geophys. Res.-Atmos. 110.
Draxler, R., Rolph, G.J.H.p., 2014. HYSPLIT (HYbrid Single-Particle Lagrangian Integrated Trajectory). Model access via NOAA ARL READY Website. http://ready.arl.noaa.gov/HYSPLIT.php.
Fan, M.Y., Zhang, Y.L., Lin, Y.C., Li, L., Xie, F., Hu, J., Mozaffar, A., Cao, F., 2021. Source apportionments of atmospheric volatile organic compounds in Nanjing, China during high ozone pollution season. Chemosphere 263, 128025.
Filley, C.M., Halliday, W., Kleinschmidt-Demasters, B.K., 2004. The effects of toluene on the central nervous system. J. Neuropathol. Exp. Neurol. 63, 1–12.
Grange, S.K., Carslaw, D.C., Lewis, A.C., Boleti, E., Hueglin, C., 2018. Random forest meteorological normalisation models for Swiss PM10 trend analysis. Atmos. Chem. Phys. 18, 6223–6239.
Guo, H., Wang, T., Louie, P.K., 2004. Source apportionment of ambient non-methane hydrocarbons in Hong Kong: application of a principal component analysis/absolute principal component scores (PCA/APCS) receptor model. Environ. Pollut. 129, 489–498.
Ho, K.F., Lee, S.C., Ho, W.K., Blake, D.R., Cheng, Y., Li, Y.S., Ho, S.S.H., Fung, K., Louie, P.K.K., Park, D., 2009. Vehicular emission of volatile organic compounds (VOCs) from a tunnel study in Hong Kong. Atmos. Chem. Phys. 9, 7491–7504.
Hsu, C.-Y., Chiang, H.-C., Shie, R.-H., Ku, C.-H., Lin, T.-Y., Chen, M.-J., Chen, N.-T., Chen, Y.-C., 2018. Ambient VOCs in residential areas near a large-scale petrochemical complex: spatiotemporal variation, source apportionment and health risk. Environ. Pollut. 240, 95–104.
Hui, L., Liu, X., Tan, Q., Feng, M., An, J., Qu, Y., Zhang, Y., Jiang, M., 2018. Characteristics, source apportionment and contribution of VOCs to ozone formation in Wuhan, Central China. Atmos. Environ. 192, 55–71.
Hui, L., Liu, X., Tan, Q., Feng, M., An, J., Qu, Y., Zhang, Y., Cheng, N., 2019. VOC characteristics, sources and contributions to SOA formation during haze events in Wuhan, Central China. Sci. Total Environ. 650, 2624–2639.
Hui, L., Liu, X., Tan, Q., Feng, M., An, J., Qu, Y., Zhang, Y., Deng, Y., Zhai, R., Wang, Z., 2020. VOC characteristics, chemical reactivity and sources in urban Wuhan, central China. Atmos. Environ. 224, 117340.
Ji, Y., Zhang, Y., Liu, D., Zhang, K., Cai, P., Zhu, B., Zhang, B., Xian, J., Wang, H., Ge, X., 2023. Using machine learning to quantify drivers of aerosol pollution trend in China from 2015 to 2022. Appl. Geochem. 151, 105614.
Kampa, M., Castanas, E., 2008. Human health effects of air pollution. Environ. Pollut. 151, 362–367.
Kelly, J.M., Doherty, R.M., O'Connor, F.M., Mann, G.W., 2018. The impact of biogenic, anthropogenic, and biomass burning volatile organic compound emissions on regional and seasonal variations in secondary organic aerosol. Atmos. Chem. Phys. 18, 7393–7422.
Kleinman, L.I., 2000. Ozone process insights from field experiments – part II: observation-based analysis for ozone production. Atmos. Environ. 34, 2023–2033.
Lau, A.K.H., Yuan, Z., Yu, J.Z., Louie, P.K.K., 2010. Source apportionment of ambient volatile organic compounds in Hong Kong. Sci. Total Environ. 408, 4138–4149.
Li, L., 2022. Development of natural gas industry in China: review and prospect. Nat. Gas Ind. B 9, 187–196.
Li, B., Hao, Y., Zhang, B., Shao, X., Hu, L., 2017a. A multifunctional noble-metal-free catalyst of CuO/TiO_2 hybrid nanofibers. Appl. Catal. A-Gen. 531, 1–12.
Li, M., Liu, H., Geng, G., Hong, C., Liu, F., Song, Y., Tong, D., Zheng, B., Cui, H., Man, H., Zhang, Q., He, K., 2017b. Anthropogenic emission inventories in China: a review. Natl. Sci. Rev. 4, 834–866.
Li, M., Zhang, Q., Zheng, B., Tong, D., Lei, Y., Liu, F., Hong, C., Kang, S., Yan, L., Zhang, Y., Bo, Y., Su, H., Cheng, Y., He, K., 2019. Persistent growth of anthropogenic non-methane volatile organic compound (NMVOC) emissions in China during 1990–2017: drivers, speciation and ozone formation potential. Atmos. Chem. Phys. 19, 8897–8913.
Li, Q., Su, G., Li, C., Liu, P., Zhao, X., Zhang, C., Sun, X., Mu, Y., Wu, M., Wang, Q., Sun, B., 2020. An investigation into the role of VOCs in SOA and ozone production in Beijing, China. Sci. Total Environ. 720, 137536.
Li, B., Ho, S.S.H., Li, X., Guo, L., Chen, A., Hu, L., Yang, Y., Chen, D., Lin, A., Fang, X., 2021. A comprehensive review on anthropogenic volatile organic compounds (VOCs) emission estimates in China: comparison and outlook. Environ. Int. 156, 106710.
Liang, S., Gao, S., Wang, S., Chai, W., Chen, W., Tang, G., 2023. Characteristics, sources of volatile organic compounds, and their contributions to secondary air pollution during different periods in Beijing, China. Sci. Total Environ. 858, 159831.
Lin, M., Holloway, T., Oki, T., Streets, D.G., Richter, A., 2009. Multi-scale model analysis of boundary layer ozone over East Asia. Atmos. Chem. Phys. 9, 3277–3301.
Liu, Y., Shao, M., Fu, L., Lu, S., Zeng, L., Tang, D., 2008. Source profiles of volatile organic compounds (VOCs) measured in China: part I. Atmos. Environ. 42, 6247–6260.
Liu, Y., Wang, H., Jing, S., Peng, Y., Gao, Y., Yan, R., Wang, Q., Lou, S., Cheng, T., Huang, C., 2021. Strong regional transport of volatile organic compounds (VOCs) during wintertime in Shanghai megacity of China. Atmos. Environ. 244, 117940.
Liu, J., Chu, B., Jia, Y., Cao, Q., Zhang, H., Chen, T., Ma, Q., Ma, J., Wang, Y., Zhang, P., He, H., 2022a. Dramatic decrease of secondary organic aerosol formation potential in Beijing: important contribution from reduction of coal combustion emission. Sci. Total Environ. 832, 155045.
Liu, Y., Qiu, P., Li, C., Li, X., Ma, W., Yin, S., Yu, Q., Li, J., Liu, X., 2022b. Evolution and variations of atmospheric VOCs and O3 photochemistry during a summer O3 event in a county-level city, Southern China. Atmos. Environ. 272, 118942.
Liu, Y., Yin, S., Zhang, S., Ma, W., Zhang, X., Qiu, P., Li, C., Wang, G., Hou, D., Zhang, X., An, J., Sun, Y., Li, J., Zhang, Z., Chen, J., Tian, H., Liu, X., Liu, L., 2024. Drivers and impacts of decreasing concentrations of atmospheric volatile organic compounds (VOCs) in Beijing during 2016–2020. Sci. Total Environ. 906, 167847.
Lv, D., Lu, S., Tan, X., Shao, M., Xie, S., Wang, L., 2021. Source profiles, emission factors and associated contributions to secondary pollution of volatile organic compounds (VOCs) emitted from a local petroleum refinery in Shandong. Environ. Pollut. 274, 116589.
Lv, Y., Tian, H., Luo, L., Liu, S., Bai, X., Zhao, H., Zhang, K., Lin, S., Zhao, S., Guo, Z.J.S.o. T.T.E., 2023. Understanding and revealing the intrinsic impacts of the COVID-19 lockdown on air quality and public health in North China using machine learning. Sci. Total Environ. 857, 159339.
Niu, Y., Yan, Y., Chai, J., Zhang, X., Xu, Y., Duan, X., Wu, J., Peng, L., 2022. Effects of regional transport from different potential pollution areas on volatile organic compounds (VOCs) in Northern Beijing during non-heating and heating periods. Sci. Total Environ. 836, 155465.
Norris, G., Duvall, R., Brown, S., Bai, S., 2014. EPA Positive Matrix Factorization (PMF) 5.0 Fundamentals and User Guide. US Environmental Protection Agency, Office of Research and Development, Washington, DC.
Nuvolone, D., Petri, D., Voller, F., 2018. The effects of ozone on human health. Environ. Sci. Pollut. Res. 25, 8074–8088.
Paatero, P., 1997. Least squares Eq.tion of robust non-negative factor analysis. Chemom. Intell. Lab. Syst. 37, 23–35.
Paatero, P., Tapper, U., 1994. Positive matrix factorization: a non-negative factor model with optimal utilization of error estimates of data values. Environmetrics 5, 111–126.
Petit, J.E., Favez, O., Albinet, A., Canonaco, F., 2017. A user-friendly tool for comprehensive evaluation of the geographical origins of atmospheric pollution: wind and trajectory analyses. Environ. Model. Softw. 88, 183–187.

Shao, P., An, J., Xin, J., Wu, F., Wang, J., Ji, D., Wang, Y., 2016. Source apportionment of VOCs and the contribution to photochemical ozone formation during summer in the typical industrial area in the Yangtze River Delta, China. Atmos. Res. 176–177, 64–74.
Shi, Z., Song, C., Liu, B., Lu, G., Xu, J., Van Vu, T., Elliott, R.J., Li, W., Bloss, W.J., Harrison, R.M.J.S.a., 2021. Abrupt but smaller than expected changes in surface air quality attributable to COVID-19 lockdowns. Nature 7, eabd6696.
Song, M., Li, X., Yang, S., Yu, X., Zhou, S., Yang, Y., Chen, S., Dong, H., Liao, K., Chen, Q., Lu, K., Zhang, N., Cao, J., Zeng, L., Zhang, Y., 2021. Spatiotemporal variation, sources, and secondary transformation potential of volatile organic compounds in Xi'an, China. Atmos. Chem. Phys. 21, 4939–4958.
Sun, W., Shao, M., Granier, C., Liu, Y., Ye, C.S., Zheng, J.Y., 2018. Long-term trends of anthropogenic SO2, NOx, CO, and NMVOCs emissions in China. Earths Future 6, 1112–1133.
van der Werf, G.R., Randerson, J.T., Giglio, L., Collatz, G.J., Mu, M., Kasibhatla, P.S., Morton, D.C., DeFries, R.S., Jin, Y., van Leeuwen, T.T., 2010. Global fire emissions and the contribution of deforestation, savanna, forest, agricultural, and peat fires (1997–2009). Atmos. Chem. Phys. 10, 11707–11735.
Vu, T.V., Shi, Z., Cheng, J., Zhang, Q., He, K., Wang, S., Harrison, R.M., 2019. Assessing the impact of clean air action on air quality trends in Beijing using a machine learning technique. Atmos. Chem. Phys. 19, 11303–11314.
Wang, Y.Q., Zhang, X.Y., Draxler, R.R., 2009. TrajStat: GIS-based software that uses various trajectory statistical analysis methods to identify potential sources from long-term air pollution measurement data. Environ. Model. Softw. 24, 938–939.
Wang, H.L., Chen, C.H., Wang, Q., Huang, C., Su, L.Y., Huang, H.Y., Lou, S.R., Zhou, M., Li, L., Qiao, L.P., Wang, Y.H., 2013. Chemical loss of volatile organic compounds and its impact on the source analysis through a two-year continuous measurement. Atmos. Environ. 80, 488–498.
Wang, M., Qin, W., Chen, W., Zhang, L., Zhang, Y., Zhang, X., Xie, X., 2020a. Seasonal variability of VOCs in Nanjing, Yangtze River delta: implications for emission sources and photochemistry. Atmos. Environ. 223.
Wang, P., Wang, T., Ying, Q., 2020b. Regional source apportionment of summertime ozone and its precursors in the megacities of Beijing and Shanghai using a source-oriented chemical transport model. Atmos. Environ. 224, 117337.
Wang, J., Yue, H., Cui, S., Zhang, Y., Li, H., Wang, J., Ge, X., 2022. Chemical characteristics and source-specific health risks of the volatile organic compounds in urban Nanjing, China. Toxics 10, 722.
Wang, B., Liu, Z., Li, Z., Sun, Y., Wang, C., Zhu, C., Sun, L., Yang, N., Bai, G., Fan, G., Sun, X., Xia, Z., Pan, G., Xu, C., Yan, G., 2023a. Characteristics, chemical transformation and source apportionment of volatile organic compounds (VOCs) during wintertime at a suburban site in a provincial capital city, east China. Atmos. Environ. 298, 119621.
Wang, Y., Cui, Y., He, Q., Fan, J., Li, Y., Liu, K., Guo, L., Wang, X., 2023b. Significant impact of VOCs emission from coking and coal/biomass combustion on O3 and SOA formation in Taiyuan, China. Atmos. Pollut. Res. 14, 101671.
Xia, L., Cai, C., Zhu, B., An, J., Li, Y., Li, Y., 2014. Source apportionment of VOCs in a suburb of Nanjing, China, in autumn and winter. J. Atmos. Chem. 71, 175–193.
Xu, R., Tang, G., Wang, Y., Tie, X., 2016. Analysis of a long-term measurement of air pollutants (2007–2011) in North China Plain (NCP); impact of emission reduction during the Beijing Olympic Games. Chemosphere 159, 647–658.
Yang, B., Zhang, Y., Qian, Y., 2012. Simulation of urban climate with high-resolution WRF model: a case study in Nanjing, China. Asia-Pac. J. Atmos. Sci. 48, 227–241.
Yang, Y., Liu, X., Zheng, J., Tan, Q., Feng, M., Qu, Y., An, J., Cheng, N., 2019. Characteristics of one-year observation of VOCs, NOx, and O3 at an urban site in Wuhan, China. J. Environ. Sci. 79, 297–310.
Yang, M., Li, F., Huang, C., Tong, L., Dai, X., Xiao, H., 2023. VOC characteristics and their source apportionment in a coastal industrial area in the Yangtze River Delta, China. J. Environ. Sci. 127, 483–494.
Yuan, B., Shao, M., Lu, S., Wang, B., 2010. Source profiles of volatile organic compounds associated with solvent use in Beijing, China. Atmos. Environ. 44, 1919–1926.
Zhan, C., Xie, M., Liu, J., Wang, T., Xu, M., Chen, B., Li, S., Zhuang, B., Li, M., 2021. Surface ozone in the Yangtze River Delta, China: a synthesis of basic features, meteorological driving factors, and health impacts. J. Geophys. Res. 126.
Zhang, Q., Streets, D.G., Carmichael, G.R., He, K.B., Huo, H., Kannari, A., Klimont, Z., Park, I.S., Reddy, S., Fu, J.S., Chen, D., Duan, L., Lei, Y., Wang, L.T., Yao, Z.L., 2009. Asian emissions in 2006 for the NASA INTEX-B mission. Atmos. Chem. Phys. 9, 5131–5153.
Zhang, Y., Wang, X., Zhang, Z., Lü, S., Shao, M., Lee, F.S.C., Yu, J., 2013. Species profiles and normalized reactivity of volatile organic compounds from gasoline evaporation in China. Atmos. Environ. 79, 110–118.
Zhang, Z., Zhang, Y., Wang, X., Lü, S., Huang, Z., Huang, X., Yang, W., Wang, Y., Zhang, Q., 2016. Spatiotemporal patterns and source implications of aromatic hydrocarbons at six rural sites across China's developed coastal regions. J. Geophys. Res. Atmos. 121, 6669–6687.
Zhang, Y., Tang, L., Croteau, P.L., Favez, O., Sun, Y., Canagaratna, M.R., Wang, Z., Couvidat, F., Albinet, A., Zhang, H., Sciare, J., Prévôt, A.S.H., Jayne, J.T., Worsnop, D.R., 2017a. Field characterization of the PM2.5 Aerosol Chemical Speciation Monitor: insights into the composition, sources, and processes of fine particles in eastern China. Atmos. Chem. Phys. 17, 14501–14517.
Zhang, Y., Tang, L., Sun, Y., Favez, O., Canonaco, F., Albinet, A., Couvidat, F., Liu, D., Jayne, J.T., Wang, Z., Croteau, P.L., Canagaratna, M.R., Zhou, H.c., Prévôt, A.S.H., Worsnop, D.R., 2017b. Limited formation of isoprene epoxydiols-derived secondary organic aerosol under NOx-rich environments in Eastern China. Geophys. Res. Lett. 44, 2035–2043.
Zhang, C., Liu, X., Zhang, Y., Tan, Q., Feng, M., Qu, Y., An, J., Deng, Y., Zhai, R., Wang, Z., Cheng, N., Zha, S., 2021a. Characteristics, source apportionment and chemical conversions of VOCs based on a comprehensive summer observation experiment in Beijing. Atmos. Pollut. Res. 12, 230–241.
Zhang, D., He, B., Yuan, M., Yu, S., Yin, S., Zhang, R., 2021b. Characteristics, sources and health risks assessment of VOCs in Zhengzhou, China during haze pollution season. J. Environ. Sci. 108, 44–57.
Zhang, D., He, B., Yuan, M., Yu, S., Yin, S., Zhang, R., 2021c. Characteristics, sources and health risks assessment of VOCs in Zhengzhou, China during haze pollution season. J. Environ. Sci. 108, 44–57.
Zhang, Z., Sun, Y., Li, J., 2023. Characteristics and sources of VOCs in a coastal city in eastern China and the implications in secondary organic aerosol and O3 formation. Sci. Total Environ. 887, 164117.
Zhao, Q., Bi, J., Liu, Q., Ling, Z., Shen, G., Chen, F., Qiao, Y., Li, C., Ma, Z., 2020. Sources of volatile organic compounds and policy implications for regional ozone pollution control in an urban location of Nanjing, East China. Atmos. Chem. Phys. 20, 3905–3919.
Zheng, J., Yu, Y., Mo, Z., Zhang, Z., Wang, X., Yin, S., Peng, K., Yang, Y., Feng, X., Cai, H., 2013. Industrial sector-based volatile organic compound (VOC) source profiles measured in manufacturing facilities in the Pearl River Delta, China. Sci. Total Environ. 456–457, 127–136.
Zheng, B., Tong, D., Li, M., Liu, F., Hong, C., Geng, G., Li, H., Li, X., Peng, L., Qi, J., Yan, L., Zhang, Y., Zhao, H., Zheng, Y., He, K., Zhang, Q., 2018. Trends in China's anthropogenic emissions since 2010 as the consequence of clean air actions. Atmos. Chem. Phys. 18, 14095–14111.
Zheng, H., Kong, S., Yan, Y., Chen, N., Yao, L., Liu, X., Wu, F., Cheng, Y., Niu, Z., Zheng, S., Zeng, X., Yan, Q., Wu, J., Zheng, M., Liu, D., Zhao, D., Qi, S., 2020. Compositions, sources and health risks of ambient volatile organic compounds (VOCs) at a petrochemical industrial park along the Yangtze River. Sci. Total Environ. 703, 135505.
Zheng, B., Zhang, Q., Geng, G., Chen, C., Shi, Q., Cui, M., Lei, Y., He, K., 2021. Changes in China's anthropogenic emissions and air quality during the COVID-19 pandemic in 2020. Earth Syst. Sci. Data 13, 2895–2907.
Zhou, W., Lei, L., Du, A., Zhang, Z., Li, Y., Yang, Y., Tang, G., Chen, C., Xu, W., Sun, J.J.J.o.G.R.A., 2022. Unexpected increases of severe haze pollution during the post COVID-19 period: effects of emissions, meteorology, and secondary production. J. Geophys. Res.-Atmos. 127, e2021JD035710.
Zou, Y., Yan, X.L., Flores, R.M., Zhang, L.Y., Yang, S.P., Fan, L.Y., Deng, T., Deng, X.J., Ye, D.Q., 2023. Source apportionment and ozone formation mechanism of VOCs considering photochemical loss in Guangzhou, China. Sci. Total Environ. 903, 166191.